INTERNATIONAL JOURNAL FOR NUMERICAL METHODS IN FLUIDS
Int. J. Numer. Meth. Fluids 2009; **61**:106–118
Published online 29 October 2008 in Wiley InterScience (www.interscience.wiley.com). DOI: 10.1002/fld.1947

Impact of the fourth-order compact difference scheme on computational properties of 3D grids in a nonhydrostatic model

Yu-di Liu[1,2,*,†], Qing-hong Zhang[2] and K. H. Lau[3]

[1]*Institute of Meteorology, PLA University of Science and Technology, Nanjing 211101, China*
[2]*Department of Atmospheric Science, School of Physics, Peking University, Beijing 100871, China*
[3]*The Institute for the Environment, The Hong Kong University and Technology, Hong Kong*

SUMMARY

To investigate the potential of the fourth-order compact difference scheme within the specific context of numerical atmospheric models, a linear baroclinic adjustment system is discretized, using a variety of candidates for practically meaningful staggered 3D grids. A unified method is introduced to derive the dispersion relationship of the baroclinic geostrophic adjustment process. Eight popular 3D grids are obtained by combining contemporary horizontal staggered grids, such as the Arakawa C and Eliassen grids, with optimal vertical grids, such as the Lorenz and Charney-Phillip (CP) grids, and their time-staggered versions. The errors produced on the 3D grids in describing the baroclinic geostrophic adjustment process relative to the differential case are compared in terms of frequency and group velocity components with the elimination of implementation error. The results show that by utilizing the fourth-order compact difference scheme with high precision, instead of the conventional second-order centered difference scheme, the errors in describing baroclinic geostrophic adjustment process decrease but only when using the combinations of the horizontally staggered Arakawa C grid and the vertically staggered CP or the C/CP grid, the time-horizontally staggered Eliassen (EL) grid and vertically staggered CP or the EL/CP grid, the C grid and the vertically time-staggered versions of Lorenz (LTS) grid or C/LTS grid, EL grid and LTS grid or EL/LTS grid. The errors were found to increase for specific waves on the rest grids. It can be concluded that errors produced on the chosen 3D grids do not universally decrease when using the fourth-order compact difference scheme; hence, care should be taken when implementing the fourth-order compact difference scheme, otherwise, the expected benefits may be offset by increased errors. Copyright © 2008 John Wiley & Sons, Ltd.

Received 2 April 2007; Revised 6 August 2008; Accepted 10 September 2008

KEY WORDS: baroclinic; geostrophic; adjustment process; compact; difference scheme; three dimension grid; fourth-order; second-order; implementation error

*Correspondence to: Yu-di Liu, Institute of Meteorology, PLA University of Science and Technology, Nanjing 211101, China.
†E-mail: yd_liu0509@yahoo.com.cn

Contract/grant sponsor: Chinese Natural Science Foundation; contract/grant number: 40505024

1. INTRODUCTION

Higher-order compact difference schemes have recently become popular in the field of computational fluid dynamics [1–5]. The aim of this work is to investigate the capability, potential and suitability of such higher-order compact difference schemes within the specific context of numerical atmospheric models. High computational costs associated with many numeric modeling projects dictate that researchers are unable to run their models on different grids with diverse difference schemes. Therefore, they have to rely on past research that explored the intricacies of combining distinct modeling components. Hopefully, this will provide the groundwork for future researchers to make informed decisions about modeling components and combinations.

The authors selected two families of schemes that are representative of commonly implemented higher- and lower-order difference schemes. The first is composed of second-order centered schemes (denoted by C2), which are the schemes traditionally used in atmospheric models [6–9]; the other is based on fourth-order compact schemes (denoted by C4), as presented, for example, in Lele [3].

As described by Fox-Rabinovitz [9] the 3D grids are obtained by combining optimal horizontal staggered grids, in this case the Arakawa C (C) and Eliassen [10] (EL) grids, with the most suitable vertical staggered grids, the Lorenz (L) and Charney-Phillip (CP) grids, and their time-staggered versions (LTS and CPTS) [11–15]. In total, eight 3D grids are considered in this work and these are abbreviated to C/L, C/CP, EL/L, EL/CP, C/LTS, C/CPTS, EL/LTS and EL/CPTS [9] in Figure 1.

In Section 2, the unified method is used to derive the dispersion properties [5] of linear baroclinic anelasticity adjustment equations by using the C2 and C4 schemes over the eight different 3D grids. Elimination of implement error is shown in Section 3. The errors in frequency, horizontal group velocity (HG) and vertical group velocity (VG) of the internal inertial gravity wave relative to the differential case (DC) on each 3D grid are compared with each other using the C2 and C4 schemes in Section 4, and finally, concluding remarks are given in Section 5.

2. COMPUTATIONAL DISPERSION PROPERTIES OF 3D GRIDS

Let us consider the simplest nonhydrostatic anelasticity system, namely, nonhydrostatic anelasticity equations [9]

$$\begin{aligned}
&\frac{\partial u}{\partial t}+\frac{\partial P}{\partial x}-fv=0\\
&\frac{\partial v}{\partial t}+\frac{\partial P}{\partial y}-fu=0\\
&\frac{\partial w}{\partial t}+\frac{\partial P}{\partial z}-g\theta=0\\
&\frac{\partial \theta}{\partial t}+Sw=0\\
&\frac{\partial u}{\partial x}+\frac{\partial v}{\partial y}+\frac{\partial w}{\partial z}=0
\end{aligned} \tag{1}$$

where u, v and w are velocity components in the x, y and z directions, respectively, $p(x,y,z,t)=\bar{p}(z)+p'(x,y,z,t)$ stands for pressure that is divided into a hydrostatic basic-state component $\bar{p}$

DOI: 10.1002/fld

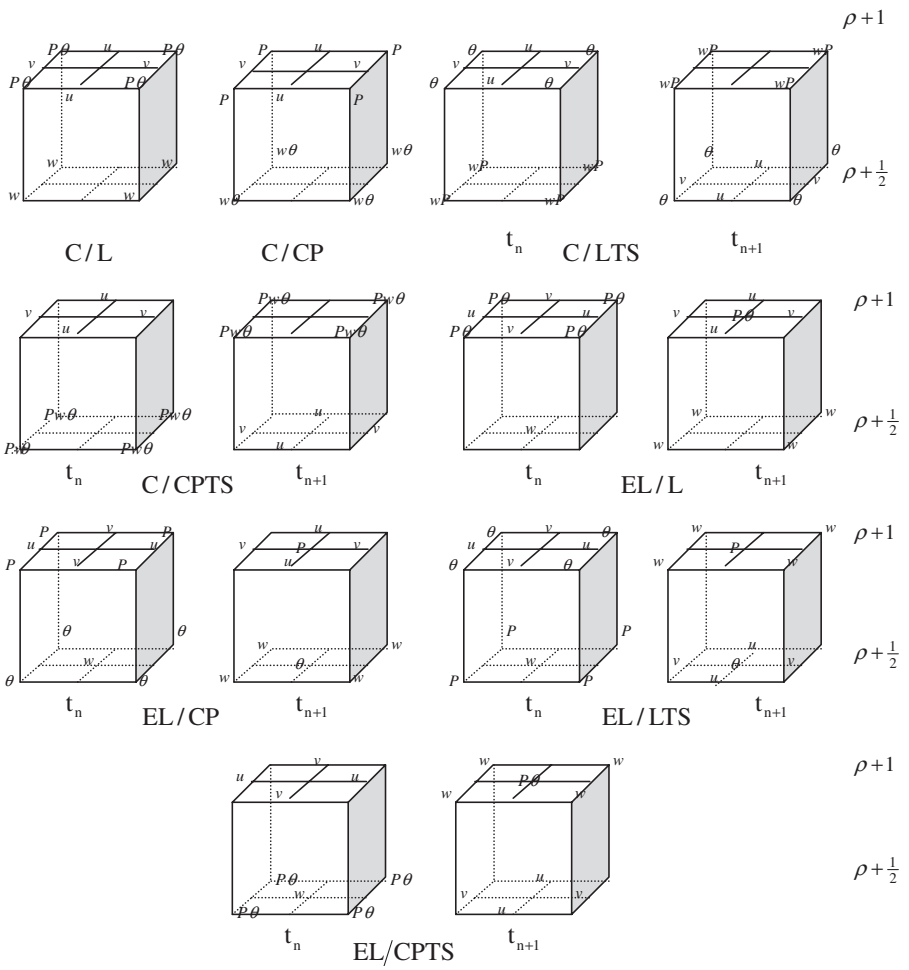

Figure 1. The variable configuration of 3D grids.

and a disturbance one p'; ρ for air density, with $P=p'/\rho_0$, the denominator being a steady ρ under Boussinesq approximation; $\Theta(x,y,z,t)=\bar{\Theta}(z)+\Theta'(x,y,z,t)$ for potential temperature, which is separated into a basic-state $\bar{\Theta}$ and a disturbance component Θ'; $S(z)=d(\ln\bar{\Theta})/\mathrm{d}z$; $\theta=\Theta'/\Theta_0$, the denominator being a steady $\bar{\Theta}$; g for gravitational acceleration; f for Coriolis force (assumed constant).

This system (1) is discretized over the C/L, C/CP, EL/L, EL/CP, C/LTS, C/CPTS, EL/LTS and EL/CPTS grids, and thus the following terms need to be approximated:

v and $\partial P/\partial x$ at a u-point,
u and $\partial P/\partial y$ at a v-point,
θ and $\partial P/\partial z$ at a w-point,
w at a θ-point, and
$\partial u/\partial x, \partial v/\partial y, \partial w/\partial z$ in the continuity equation.

DOI: 10.1002/fld

We first define the following operators: operator $\hat{R}_0$ denotes an approximation of $v(u)$ at a $u(v)$ gridpoint; $\hat{H}_0$, an approximation of $w(\theta)$ at a $\theta(w)$ gridpoint; $\hat{K}$, an approximation of $\partial P/\partial x$ at a u gridpoint; $\hat{L}$, an approximation of $\partial P/\partial y$ at a v gridpoint; $\hat{M}$, an approximation of $\partial P/\partial z$ at a w gridpoint, and $\hat{K}+\hat{L}+\hat{M}$, an approximation of $\partial u/\partial x+\partial v/\partial y+\partial w/\partial z$ in the continuity equation, which is the same on all grids. For the eight grids the representations of the operators are listed in Table I.

Setting $(\hat{R}_0, \hat{H}_0, \hat{K}, \hat{L}, \hat{M}) = (R_0, H_0, K, L, M)\mathrm{e}^{\mathrm{i}(kx+ly+mz)}$, where k, l and m are the wavenumbers in the x, y and z directions, respectively. Then, the operator R_0, H_0 can be deduced from the $\hat{R}_0, \hat{H}_0$ in Table I (refer to Table II for details). $\hat{K}, \hat{L}$ and $\hat{M}$ on all eight grids are estimates of the first derivative at the midpoints and are listed in Table III. The operators K, L, M, deduced from $\hat{K}, \hat{L}, \hat{M}$, are listed in Table IV in detail.

Using the operators mentioned above, Equation (1) with $\Delta t \to 0$ is semi-discretized as:

$$\frac{\partial u}{\partial t} + \hat{K}(P) - f\hat{R}_0(v) = 0$$

$$\frac{\partial v}{\partial t} + \hat{L}(P) + f\hat{R}_0(u) = 0$$

Table I. $\hat{R}_0$ and $\hat{H}_0$ on grids C/L, C/CP, EL/L, EL/CP, C/LTS, C/CPTS, EL/LTS, EL/CPTS and differential case (DC).

	C/L	C/CP	EL/L	EL/CP	DC
$\hat{R}_0$	$\bar{R}^x\bar{R}^y$	$\bar{R}^x\bar{R}^y$	(a)	(a)	(a)
$\hat{H}_0$	$\bar{R}^z$	(a)	$\bar{R}^z$	(a)	(a)
	C/LTS	C/CPTS	EL/LTS	EL/CPTS	
$\hat{R}_0$	$\bar{R}^x\bar{R}^y\bar{R}^z$	$\bar{R}^x\bar{R}^y\bar{R}^z$	$\bar{R}^z$	$\bar{R}^z$	
$\hat{H}_0$	(a)	$\bar{R}^z$	(a)	$\bar{R}^z$	

Note: $\bar{R}^x, \bar{R}^y$ and $\bar{R}^z$ denote the average operator in x, y and z directions, respectively, (refer to Table III for details), (a) denotes the exact solution.

Table II. Operators R_0 and H_0 on grids C/L, C/CP, EL/L, EL/CP, C/LTS, C/CPTS, EL/LTS, EL/CPTS and differential case (DC).

	C/L	C/CP	EL/L	EL/CP
R_0	$T_0(k)T_0(l)$	$T_0(k)T_0(l)$	1	1
H_0	$T_0(m)$	1	$T_0(m)$	1
	C/LTS	C/CPTS	EL/CPTS	EL/LTS	DC
R_0	$T_0(k)T_0(l)T_0(m)$	$T_0(k)T_0(l)T_0(m)$	$T_0(m)$	$T_0(m)$	1
H_0	1	$T_0(m)$	$T_0(m)$	1	1

DOI: 10.1002/fld

Table III. Average operators $\bar{R}^x$, $\bar{R}^y$, $\bar{R}^z$ and difference operators $\hat{K}$, $\hat{L}$ and $\hat{M}$ of C2 and C4 [5].

Operator	Concrete expression
C2	
$\bar{R}^x$	$f_{\kappa+1/2,\mu,\rho}=(f_{\kappa,\mu,\rho}+f_{\kappa+1,\mu,\rho})/2$
$\bar{R}^y$	$f_{\kappa,\mu+1/2,\rho}=(f_{\kappa,\mu,\rho}+f_{\kappa,\mu+1,\rho})/2$
$\bar{R}^z$	$f_{\kappa,\mu,\rho+1/2}=(f_{\kappa,\mu,\rho}+f_{\kappa,\mu,\rho+1})/2$
$\hat{K}$	$f'_{\kappa+1/2,\mu,\rho}=(f_{\kappa+1,\mu,\rho}-f_{\kappa,\mu,\rho})/\Delta x$
$\hat{L}$	$f'_{\kappa,\mu+1/2,\rho}=(f_{\kappa,\mu+1,\rho}-f_{\kappa,\mu,\rho})/\Delta y$
$\hat{M}$	$f'_{\kappa,\mu,\rho+1/2}=(f_{\kappa,\mu,\rho+1}-f_{\kappa,\mu,\rho})/\Delta z$
C4	
$\bar{R}^x$	$\frac{1}{6}f_{\kappa-1/2,\mu,\rho}+f_{\kappa+1/2,\mu,\rho}+\frac{1}{6}f_{\kappa+3/2,\mu,\rho}=\frac{2}{3}(f_{\kappa,\mu,\rho}+f_{\kappa+1,\mu,\rho})$
$\bar{R}^y$	$\frac{1}{6}f_{\kappa,\mu-1/2,\rho}+f_{\kappa,\mu+1/2,\rho}+\frac{1}{6}f_{\kappa,\mu,\rho+3/2}=\frac{2}{3}(f_{\kappa,\mu,\rho}+f_{\kappa,\mu+1,\rho})$
$\bar{R}^z$	$\frac{1}{6}f_{\kappa,\mu,\rho-1/2}+f_{\kappa,\mu,\rho+1/2}+\frac{1}{6}f_{\kappa,\mu,\rho+3/2}=\frac{2}{3}(f_{\kappa,\mu,\rho}+f_{\kappa,\mu,\rho+1})$
$\hat{K}$	$\frac{1}{22}f'_{\kappa-1/2,\mu,\rho}+f'_{\kappa+1/2,\mu,\rho}+\frac{1}{22}f'_{\kappa+3/2,\mu,\rho}=\frac{12}{11}\frac{f_{\kappa+1,\mu,\rho}-f_{\kappa,\mu,\rho}}{\Delta x}$
$\hat{L}$	$\frac{1}{22}f'_{\kappa,\mu-1/2,\rho}+f'_{\kappa,\mu+1/2,\rho}+\frac{1}{22}f'_{\kappa,\mu+3/2,\rho}=\frac{12}{11}\frac{f_{\kappa,\mu+1,\rho}-f_{\kappa,\mu,\rho}}{\Delta y}$
$\hat{M}$	$\frac{1}{22}f'_{\kappa,\mu,\rho-1/2}+f'_{\kappa,\mu,\rho+1/2}+\frac{1}{22}f'_{\kappa,\mu,\rho+3/2}=\frac{12}{11}\frac{f_{\kappa,\mu,\rho+1}-f_{\kappa,\mu,\rho}}{\Delta z}$

Note that $f_{\kappa,\mu,\rho}$ denotes the variable f at gridpoint $(x_\kappa, y_\mu, z_\rho)$; then, operator $\bar{R}^x$ represents the approximation $f_{\kappa+1/2,\mu,\rho}$ of variable f at the mid-gridpoints $(x_{\kappa+1/2}, y_\mu, z_\rho)$; operator $\hat{K}$ the approximation $f'_{\kappa+1/2,\mu,\rho}$ of the first-order derivative f' of variable f at mid-gridpoints $(x_{\kappa+1/2}, y_\mu, z_\rho)$; operators $\bar{R}^y$ and $\bar{R}^z$ ($\hat{L}$ and $\hat{M}$) are similar to $\bar{R}^x$ ($\hat{K}$) except in the different direction.

$$\begin{aligned}\frac{\partial w}{\partial t}+\hat{M}(P)-g\hat{H}_0(\theta)=0\\ \frac{\partial \theta}{\partial t}+S\hat{H}_0(w)=0\\ \hat{K}(u)+\hat{L}(v)+\hat{M}(w)=0\end{aligned} \tag{2}$$

Setting wave solutions

$$(u, v, w, P, \theta)=(\bar{U}, \bar{V}, \bar{W}, \bar{P}, \bar{\Theta})\mathrm{e}^{\mathrm{i}(k\kappa\Delta x+l\mu\Delta y+m\rho\Delta z-n\omega\Delta t)} \tag{3}$$

where κ, μ, ρ and n are serial numbers (positive integers) of x-, y-, z- and t-dimensions, respectively. ω is the frequency.

Substituting wave solution (3) into Equation (2), and considering the abovementioned operators, we get the following form of Equation (2) with $\Delta t \to 0$:

$$\begin{aligned}-\mathrm{i}\omega\bar{U}+K\bar{P}-f\bar{V}R_0=0\\ -\mathrm{i}\omega\bar{V}+L\bar{P}+f\bar{U}R_0=0\end{aligned}$$

DOI: 10.1002/fld

Table IV. Operators $T_0(k), T_0(l), T_0(m), K, L$ and M of C2, C4 and differential case [5].

Operator	Concrete expression
Differential case derivative	
	$K = \mathrm{i}k$
	$L = \mathrm{i}l$
	$M = \mathrm{i}m$
C2	
	$T_0(k) = \cos\frac{k\Delta x}{2}$
	$T_0(l) = \cos\frac{l\Delta y}{2}$
	$T_0(m) = \cos\frac{m\Delta z}{2}$
	$K = \frac{2\mathrm{i}}{\Delta x}\sin\frac{k\Delta x}{2}$
	$L = \frac{2\mathrm{i}}{\Delta y}\sin\frac{l\Delta y}{2}$
	$M = \frac{2\mathrm{i}}{\Delta z}\sin\frac{m\Delta z}{2}$
C4	
	$T_0(k) = \frac{4\cos(k\Delta x/2)}{3+\cos k\Delta x}$
	$T_0(l) = \frac{4\cos(l\Delta y/2)}{3+\cos l\Delta y}$
	$T_0(m) = \frac{4\cos(m\Delta z/2)}{3+\cos m\Delta z}$
	$K = \frac{2\mathrm{i}}{\Delta x} \times \frac{12\sin(k\Delta x/2)}{11+\cos k\Delta x}$
	$L = \frac{2\mathrm{i}}{\Delta y} \times \frac{12\sin(l\Delta y/2)}{11+\cos l\Delta y}$
	$M = \frac{2\mathrm{i}}{\Delta z} \times \frac{12\sin(m\Delta z/2)}{11+\cos m\Delta z}$

$$-\mathrm{i}\omega\bar{W} + M\bar{P} - g\bar{\Theta}H_0 = 0$$

$$-\mathrm{i}\omega\bar{\Theta} + S\bar{W}H_0 = 0$$

$$K\bar{U} + L\bar{V} + M\bar{W} = 0$$

Hence the dispersion relationship is solved as:

$$\left(\frac{\omega}{f}\right)^2 = \frac{R_0^2 M^2 + \lambda^2(K^2+L^2)H_0^2}{K^2+L^2+M^2} \tag{4}$$

Here $\lambda = \sqrt{gS}/f$, a dimensionless parameter, is the ratio of the Brunt-Vaisala frequency to the Coriolis parameter.

Subsequently, substituting the operators from Table II into Equation (4), the dispersion relationships on the grids are extracted (see Table V for details).

The operators $T_0(k), T_0(l), T_0(m), K, L$ and M of C2, C4 and the DC in Table IV are substituted into Table V and the dispersion relationships using C2 and C4 on the grids can be obtained (in Table VI using C2 and in Table VII using C4).

DOI: 10.1002/fld

Table V. Dispersion relationships on grids C/L, C/CP, EL/L, EL/CP, C/LTS, C/CPTS, EL/LTS, EL/CPTS and differential case (DC).

Grid	Dispersion relationship
C/L	$\left(\frac{\omega}{f}\right)^2=\frac{T_0^2(k)T_0^2(l)M^2+\lambda^2T_0^2(m)(K^2+L^2)}{K^2+L^2+M^2}$
C/CP	$\left(\frac{\omega}{f}\right)^2=\frac{T_0^2(k)T_0^2(l)M^2+\lambda^2(K^2+L^2)}{K^2+L^2+M^2}$
EL/L	$\left(\frac{\omega}{f}\right)^2=\frac{M^2+\lambda^2(K^2+L^2)T_0^2(m)}{K^2+L^2+M^2}$
EL/CP	$\left(\frac{\omega}{f}\right)^2=\frac{M^2+\lambda^2(K^2+L^2)}{K^2+L^2+M^2}$
C/LTS	$\left(\frac{\omega}{f}\right)^2=\frac{T_0^2(k)T_0^2(l)T_0^2(m)M^2+\lambda^2(K^2+L^2)}{K^2+L^2+M^2}$
C/CPTS	$\left(\frac{\omega}{f}\right)^2=\frac{T_0^2(k)T_0^2(l)T_0^2(m)M^2+\lambda^2(K^2+L^2)T_0^2(m)}{K^2+L^2+M^2}$
EL/LTS	$\left(\frac{\omega}{f}\right)^2=\frac{T_0^2(m)M^2+\lambda^2(K^2+L^2)}{K^2+L^2+M^2}$
EL/CPTS	$\left(\frac{\omega}{f}\right)^2=\frac{T_0^2(m)M^2+\lambda^2(K^2+L^2)T_0^2(m)}{K^2+L^2+M^2}$
DC	$\left(\frac{\omega}{f}\right)^2=\frac{m^2+\lambda^2(k^2+l^2)}{k^2+l^2+m^2}$

HG and VG are derived from the dispersion equation

$$\mathrm{HG}=\partial\omega/\partial k,\quad VG=\partial\omega/\partial m$$

They will be compared using graphic representations in Section 3.

3. ELIMINATION OF THE IMPLEMENTATION ERROR

To ensure no implementation error before the analysis of errors in frequency, HG and VG of the internal inertial gravity wave relative to the DC on each 3D grid using the C2 and C4 schemes, at first the consistency is measured [16–18]. When $\Delta x, \Delta y$ and Δz go to zero then every dispersion relationship in Tables VI and VII approaches the DC in Table V, i.e. the dispersion relationships in Tables VI and VII are mistake-free. Second, in the process of plotting the Figures 2–4 in the next section, all figures are plotted by a software such as Matlab™ and Maple ™, respectively, and the resulting figures are same. Hence there are no implementation errors in the results.

4. DISCUSSION OF COMPUTATIONAL DISPERSION PROPERTIES

For simplicity, we assume that the horizontal intervals and wavenumbers are equal: $\Delta x=\Delta y$ and $k=l$. This indicates that only the x-axis component is given in Figures 2–4.

DOI: 10.1002/fld

Table VI. Dispersion relationships on 3D grids using C2.

Grid	Dispersion relationship
C/L	$\left(\frac{\omega}{f}\right)^2=\frac{\Re_1\cos^2\frac{k\Delta x}{2}\cos^2\frac{l\Delta y}{2}+\lambda^2\Re_2\cos^2\frac{m\Delta z}{2}}{\Re_1+\Re_2}$
C/CP	$\left(\frac{\omega}{f}\right)^2=\frac{\Re_1\cos^2\frac{k\Delta x}{2}\cos^2\frac{l\Delta y}{2}+\lambda^2\Re_2}{\Re_1+\Re_2}$
EL/L	$\left(\frac{\omega}{f}\right)^2=\frac{\Re_1+\lambda^2\Re_2\cos^2\frac{m\Delta z}{2}}{\Re_1+\Re_2}$
EL/CP	$\left(\frac{\omega}{f}\right)^2=\frac{\Re_1+\lambda^2\Re_2}{\Re_1+\Re_2}$
C/LTS	$\left(\frac{\omega}{f}\right)^2=\frac{\Re_1\cos^2\frac{k\Delta x}{2}\cos^2\frac{l\Delta y}{2}\cos^2\frac{m\Delta z}{2}+\lambda^2\Re_2}{\Re_1+\Re_2}$
C/CPTS	$\left(\frac{\omega}{f}\right)^2=\frac{\Re_1\cos^2\frac{k\Delta x}{2}\cos^2\frac{l\Delta y}{2}\cos^2\frac{m\Delta z}{2}+\lambda^2\Re_2\cos^2\frac{m\Delta z}{2}}{\Re_1+\Re_2}$
EL/LTS	$\left(\frac{\omega}{f}\right)^2=\frac{\Re_1\cos^2\frac{m\Delta z}{2}+\lambda^2\Re_2}{\Re_1+\Re_2}$
EL/CPTS	$\left(\frac{\omega}{f}\right)^2=\frac{\Re_1\cos^2\frac{m\Delta z}{2}+\lambda^2\Re_2\cos^2\frac{m\Delta z}{2}}{\Re_1+\Re_2}$

Where $\Re_1=\left(\sin\frac{m\Delta z}{2}\Big/(\Delta z/2)\right)^2$, $\Re_2=\left(\sin\frac{k\Delta x}{2}\Big/(\Delta x/2)\right)^2+\left(\sin\frac{l\Delta y}{2}\Big/(\Delta y/2)\right)^2$.

In this section the grid spacing is set at $\Delta x=100\,\mathrm{m}$, $\Delta z=100\,\mathrm{m}$ [19] and for the dimensionless parameter $\lambda=100$.

In order to account for the difference between the discretized solutions on the grids and the DC, the relative error R of frequency, HG or VG is compared, in which R is defined by

$$R_j^i=\frac{C_j^i-C_j^{\mathrm{diff}}}{C_j^{\mathrm{diff}}}$$

Here the superscript i denotes the discretized solution, diff denotes the DC and the subscript j denotes frequency, HG or VG.

The relative errors of frequency on the eight 3D grids using the C2 and C4 schemes are given in Figure 2. For the C/CP, EL/CP, C/LTS and EL/LTS grids, the errors show the same distributive pattern; the maximal errors are around 50% for C2 scheme and drop to 20% for C4 scheme. But, for the C/L, EL/L, C/LTS, EL/LTS grids, though the maximal relative errors maintain the same value of 100%, for a given vertical wavenumber the errors for C4 are less than those for C2. In general, with regard to frequency when moving to a higher-order difference scheme, for every grid the relative errors decrease.

The relative errors of HG on each grid using C2 and C4 schemes are displayed in Figure 3. For the C/L, EL/L, C/CPTS and EL/CPTS grids the domain of accuracy is much enlarged when using the C4 scheme in comparison with the C2 scheme, though the maximal errors remain unchanged. The positive maximal relative errors on C/CP, EL/CP, C/LTS and EL/LTS grids is 50% and 20% for the C2 and C4 schemes, respectively, whereas the negative maximal relative

DOI: 10.1002/fld

Table VII. Dispersion relationships on 3D grids using C4.

Grid	Dispersion relationship
C/L	$\left(\frac{\omega}{f}\right)^2=\frac{\aleph_1 A(k\Delta x)A(l\Delta y)+\lambda^2\aleph_2 A(m\Delta z)}{\aleph_1+\aleph_2}$
C/CP	$\left(\frac{\omega}{f}\right)^2=\frac{\aleph_1 A(k\Delta x)A(l\Delta y)+\lambda^2\aleph_2}{\aleph_1+\aleph_2}$
EL/L	$\left(\frac{\omega}{f}\right)^2=\frac{\aleph_1+\lambda^2\aleph_2 A(m\Delta z)}{\aleph_1+\aleph_2}$
EL/CP	$\left(\frac{\omega}{f}\right)^2=\frac{\aleph_1+\lambda^2\aleph_2}{\aleph_1+\aleph_2}$
C/LTS	$\left(\frac{\omega}{f}\right)^2=\frac{\aleph_1 A(k\Delta x)A(l\Delta y)A(m\Delta z)+\lambda^2\aleph_2}{\aleph_1+\aleph_2}$
C/CPTS	$\left(\frac{\omega}{f}\right)^2=\frac{\aleph_1 A(k\Delta x)A(l\Delta y)A(m\Delta z)+\lambda^2\aleph_2 A(m\Delta z)}{\aleph_1+\aleph_2}$
EL/LTS	$\left(\frac{\omega}{f}\right)^2=\frac{\aleph_1 A(m\Delta z)+\lambda^2\aleph_2}{\aleph_1+\aleph_2}$
EL/CPTS	$\left(\frac{\omega}{f}\right)^2=\frac{\aleph_1 A(m\Delta z)+\lambda^2\aleph_2 A(m\Delta z)}{\aleph_1+\aleph_2}$

Where $\aleph_1=\left(\frac{12\sin(m\Delta z/2)}{11+\cos m\Delta z}\times\frac{2}{\Delta z}\right)^2$, $\aleph_2=\left(\frac{12\sin(k\Delta x/2)}{11+\cos k\Delta x}\times\frac{2}{\Delta x}\right)^2+\left(\frac{12\sin(l\Delta y/2)}{11+\cos l\Delta y}\times\frac{2}{\Delta y}\right)^2$,
$A(k\Delta x)=\left(\frac{4\cos(k\Delta x/2)}{3+\cos k\Delta x}\right)^2$, $A(l\Delta x)=\left(\frac{4\cos(l\Delta x/2)}{3+\cos l\Delta y}\right)^2$, $A(m\Delta z)=\left(\frac{4\cos(m\Delta z/2)}{3+\cos m\Delta z}\right)^2$.

errors for the C4 scheme are the same as for the C2 scheme of 100%. When $m\Delta z$ is close to π, for a given horizontal wavenumber the relative errors of HG for C4 are less than that for C2; while, if $m\Delta z$ is close to zero, for a given horizontal wavenumber the relative errors of HG for C4 are the same as those for C2. With regard to HG, relative errors on 3D grids have not shown uniform decrease when the traditional C2 scheme is replaced by the C4 scheme.

The relative errors of VG on each of the grid combinations using the C2 and C4 schemes are shown in Figure 4. The negative maximal relative errors when using the C4 scheme are the same values as the those of the C2 scheme of approximately 80% for the C/CP, EL/CP, C/LTS and EL/LTS grids. The positive maximal error for the C4 scheme is 60%, which is the half value for C2 (120%). When $m\Delta z$ is close to zero and $k\Delta x$ is close to π, the improvement of the high-order scheme over the conventional scheme is obvious. Conversely, on the C/L and EL/L grids, the maximal relative error for the C4 scheme is 800%, which is higher than that for C2 scheme (600%). Furthermore, when $m\Delta z$ is close to π and $k\Delta x$ is close to π, the relative errors when using the C4 scheme swell to 800%, which is more than twice the error of the C2 scheme (350%). For the C/CPTS and EL/CPTS grids the change of error is similar to that for the C/L and EL/L grids when the C2 scheme is replaced by the C4 scheme. Overall, with respect to the VG, when the differential scheme is upgraded to the fourth-order compact scheme from the second-order center-differential scheme, obvious improvement is shown only on the C/CP, EL/CP, C/LTS and EL/LTS grids. The errors increase on the C/L, EL/L, C/CPTS and EL/CPTS grids for short waves in both vertical and horizontal directions.

DOI: 10.1002/fld

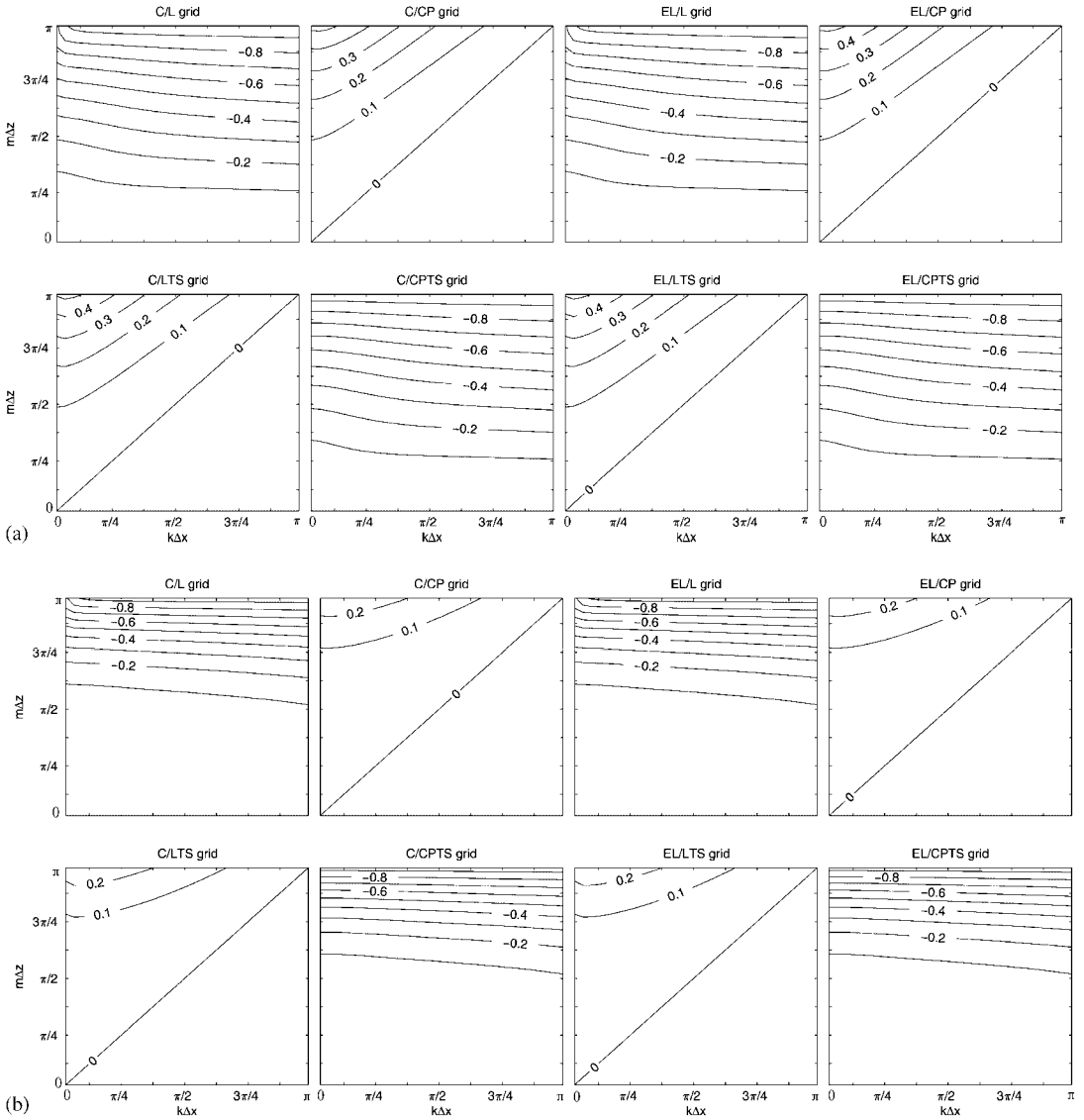

Figure 2. The relative errors of frequency on 3D grids by using C2 (a) and C4 (b).

It was found that, in general, using the fourth-order compact difference scheme with high precision instead of the conventional second-order centered difference scheme, for the chosen eight 3D grids, will not universally decrease the error. The improvement is obvious only on C/CP, EL/CP, C/LTS and EL/LTS grids, while the errors increase in specific waves on other grids.

This can be easily explained by the form of the discrete dispersion relationship (in Table V) since the frequency appears as a ratio, and improving both the numerator and the denominator of (in Table V) will not necessarily improve the ratio itself, so do the HG and VG.

DOI: 10.1002/fld

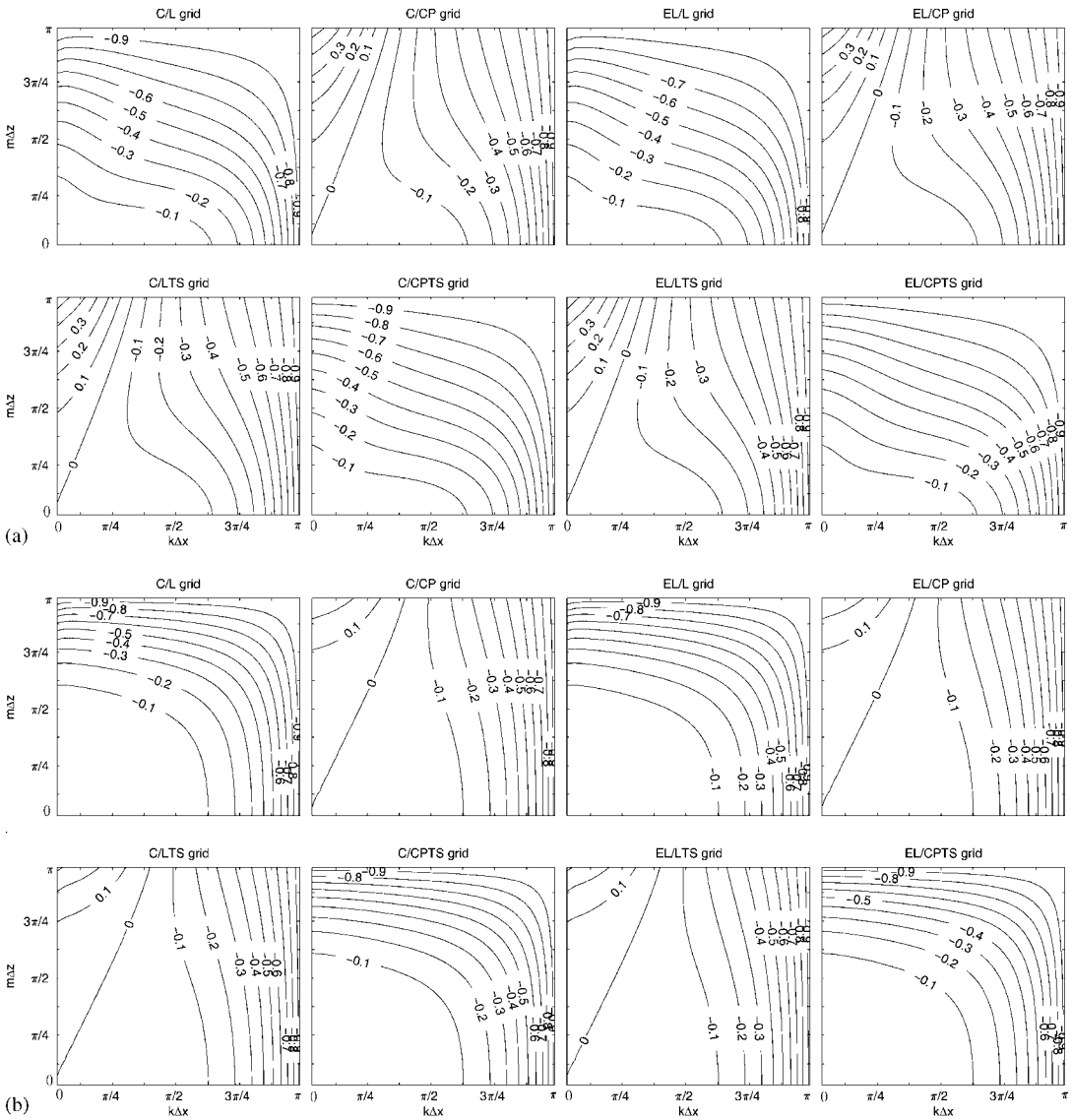

Figure 3. The relative errors of HG on 3D grids by using C2 (a) and C4 (b).

5. CONCLUSIONS

To understand the capability, potential and suitability of fourth-order compact difference schemes within the specific context of numerical atmospheric models, the linear baroclinic adjustment equations in a nonhydrostatic case are considered and discretized on eight different 3D grids with a combination of the horizontally staggered Arakawa C and the time-horizontally staggered Eliassen

DOI: 10.1002/fld

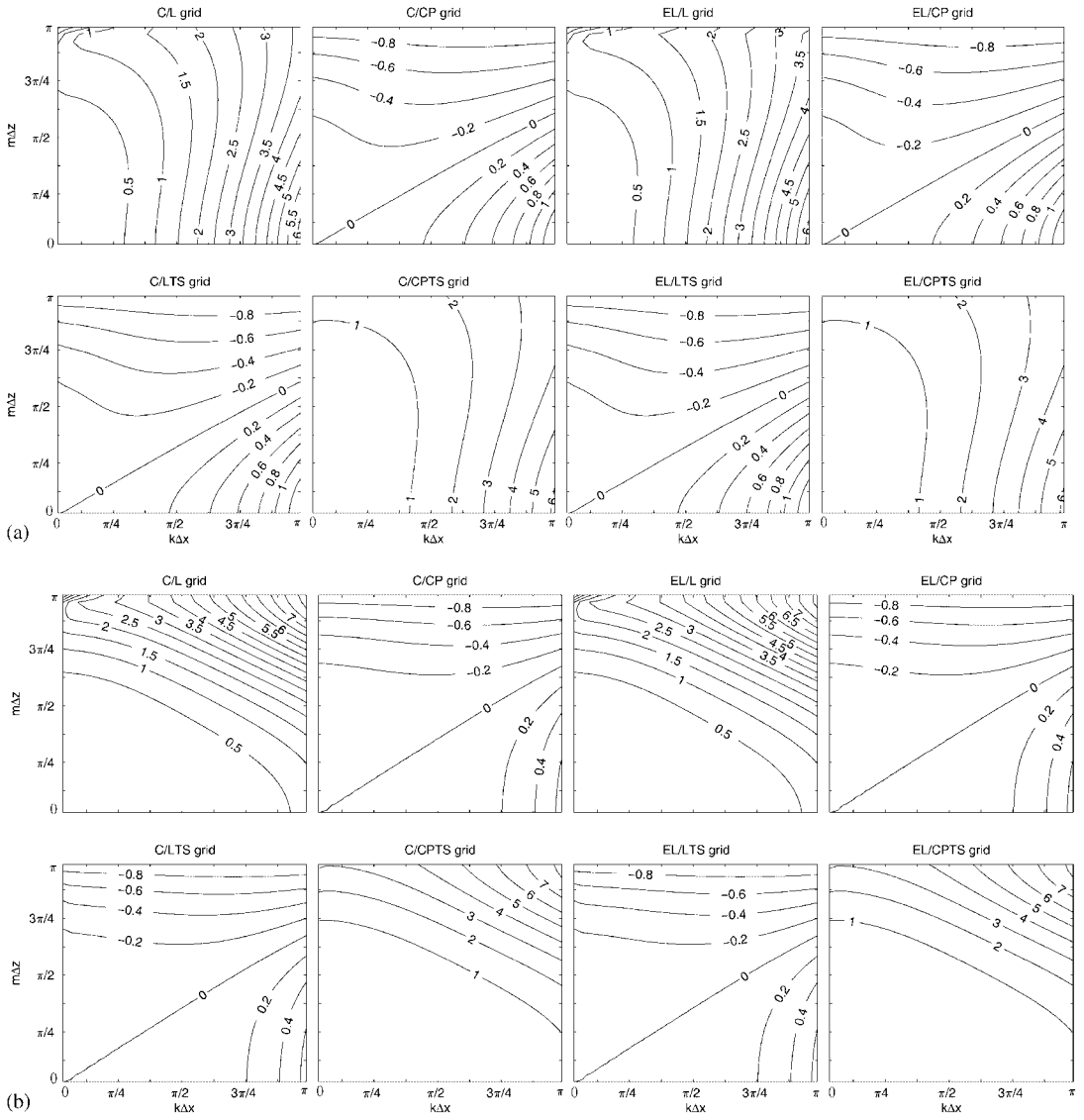

Figure 4. The relative errors of VG on 3D grids by using C2 (a) and C4 (b).

(EL) grids and vertically staggered L, CP, LTS and CPTS grids. The unified method is introduced to deduce the dispersion relationship by C2 and C4 schemes on the above grids.

With regard to the linear baroclinic adjustment equations, the errors of frequency, HG and VG relative to the DC for the C4 scheme are compared with those for the C2 scheme with the elimination of the implementation error. If the 3D grid is a staggered C or EL grid in the horizontal and an L or CPTS staggered grid in the vertical directions, upgrading the difference scheme from second order to the fourth order will decrease the precision of the model. If the 3D grid is a

DOI: 10.1002/fld

staggered C or EL grid in the horizontal direction and CP or LTS staggered grid in the vertical direction, model precision will be increased.

The errors produced on the specific 3D grids cannot universally decrease by using the C4 scheme, and care should be taken where the C4 scheme is utilized; otherwise, the expected benefits may be eroded by increased errors.

Of course, the conclusions are gained on the basis of the linear equations, but in the case of nonlinear baroclinic primitive equations, in particular after considering the more perfect physical process, what is the result? They need to be further studied in the future.

REFERENCES

1. Zingg DW, Lomax H, Jurgens H. High-accuracy finite-difference schemes for linear wave propagation. *SIAM Journal on Scientific Computing* 1996; **17**(2):328–346.
2. Adam Y. Highly accurate compact implicit methods and boundary conditions. *Journal of Computational Physics* 1977; **24**:10–22.
3. Lele SK. Compact finite difference schemes with spectral-like resolution. *Journal of Computational Physics* 1992; **103**:16–42.
4. Chu PC, Fan C. A three-point combined compact difference scheme. *Journal of Computational Physics* 1998; **140**:370–399.
5. Blayo E. Compact finite difference schemes for ocean models. *Journal of Computational Physics* 2000; **164**: 241–257.
6. Collatz L. *The Numerical Treatment of Differential Equations*. Springer: New York, 1966; 263–296.
7. Rondall DA. Geostrophic adjustment and the finite difference shallow water equations. *Monthly Weather Review* 1994; **122**:1371–1377.
8. Song Y, Tang T. Dispersion and group velocity in numerical schemes for three-dimensional hydrodynamic equation. *Journal of Computational Physics* 1993; **105**:72–82.
9. Fox-Rabinovitz MS. Computational dispersion properties of 3D staggered grids for a nonhydrostatic anelastic system. *Monthly Weather Review* 1996; **124**:498–510.
10. Eliassen A. A procedure for numerical integration of the primitive equations of the two-parameter model of the atmosphere. *Scientific Report No. 4*, Department of Meteorology, UCLA, 1956; 1–56.
11. Wajsowicz RC. Free planetary waves in finite-difference numerical models. *Journal of Physical Oceanography* 1986; **16**:773–789.
12. Adcroft AJ. Numerical algorithms for use in a dynamical model of the ocean. *Ph.D. Thesis*, University of London, 1995.
13. Dukowicz JK. Mesh effects for Rossby waves. *Journal of Computational Physics* 1995; **119**:188–192.
14. Winninghoff FJ. On the adjustment toward a geostrophic balance in a simple primitive equation model with application to the problems of initialization and objective analysis. *Thesis*, University of California, LA, 1968; 1–156.
15. Arakawa A, Lamb VR. Computational design of the basic dynamical processes of the UCLA general circulation model. *Methods in Computational Physics* 1977; **17**:173–265.
16. Roache PJ. Verification of codes and calculations. *AIAA Journal* 1998; **36**:696–702.
17. Roy CJ, Nelson CC, Smith TM, Ober CC. Verification of Euler/Navier–Stokes codes using the method of manufactured solutions. *International Journal for Numerical Methods in Fluids* 2004; **44**(6):599–620.
18. Roy CJ. Review of code and solution verification procedures for computational simulation. *Journal of Computational Physics* 2005; **205**:131–156.
19. Straka JM, Wilhelmson RB, Wicker LJ, Anderson JR, Droegemeier KK. Numerical solutions of a non-linear density current: a benchmark solution and comparisons. *International Journal for Numerical Methods in Fluids* 1993; **17**:1–22.

DOI: 10.1002/fld